Proceedings of the ASME 2025
International Design Engineering Technical Conference
IDETC2025
August 17–20, 2025, Anaheim, CA

IDETC2025-168835

COMPUTER VISION-BASED IN-SITU MONITORING OF COOPERATIVE 3D PRINTING IN A CLOSED-LOOP SYSTEM

Harshin Sanam, Anuj Swaminathan, Zhenghui Sha*

Walker Department of Mechanical Engineering
The University of Texas at Austin
Austin, TX, USA

ABSTRACT

Cooperative 3D printing (C3DP) is an emerging field in Swarm Manufacturing (SM) that allows larger format objects to be printed in parallel for improved efficiency without compromising print quality. Our previous work with in-situ monitoring of C3DP includes detecting stringing defects and 2D image matching in fused filament fabrication 3D printing. However, the lack of true in-situ analysis impeded proper closed-loop control. In this study, we improve the in-situ monitoring framework by utilizing the Canny edge detection used for 2D image matching in our previous work to detect warping, layer splitting, and interstitial gaps. After testing four different methods, including bounding edge comparison, closest point comparison, corner point comparison, and K-nearest neighbor regression comparison, we were able to accurately measure warping effects using corner points of the detected contours. This corner point comparison method can effectively determine the severity of warping, allowing us to have closed-loop control of a heated bed that can successfully decrease warping effects. The proposed methods can also detect interstitial gaps on a y-axis basis, and continuously collect data to communicate G-code commands to the printers for recalibration and stopping fatal prints. The computer vision-based monitoring framework presented in this paper laid a good foundation to improve the C3DP process and provided insight into the in-situ monitoring of various other forms of additive manufacturing.

Keywords: Additive Manufacturing, In-Situ Monitoring, Closed-Loop Control, Cooperative 3D Printing, Defect Detection

1. INTRODUCTION

Additive Manufacturing (AM) technologies have not only advanced in their applications, but have also developed in their methodologies as it pertains to process improvements. The single printer for fused filament fabrication (FFF) has existed for many years, but a big limitation to this manufacturing process is that the workflow efficiency is limited by the deposition rate and the print area (e.g., limited by one nozzle and fixed build volume) as well as the trade-off between these two factors and print quality and cost. Cooperative 3D printing (C3DP) addresses these issues as an emerging technology in the realm of Swarm Manufacturing (SM) by utilizing multiple mobile robotic printers on a fully open, modular factory floor. C3DP harnesses the ability of multiple robotic arms to cooperatively 3D print parts in an optimized way compared to gantry based systems that follow a conventional axis oriented printing. This robotic arm technology is the future for larger 3D printing across various materials and methods (e.g. wire arc, cold spray, and FDM.

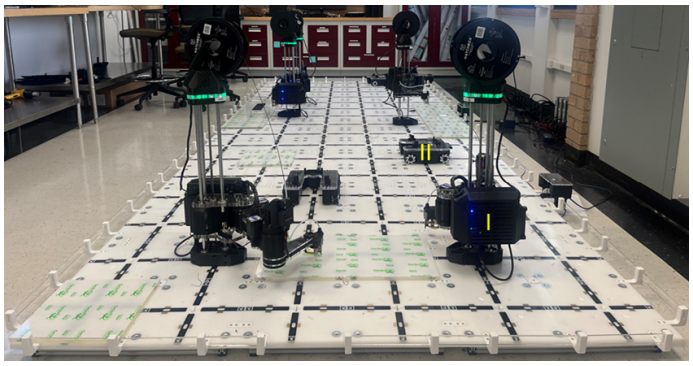

FIGURE 1: C3DP PLATFORM [1]. (I) SCARA PRINTING ROBOT AND (II) MOBILE TRANSPORTER ROBOT

The C3DP system, as shown in Figure 1, is a grid of tiles that have slots for printers and other robots. The printers utilize a Selective Compliance Articulated Robot Arm (SCARA) design that is secured to the slots on the floor and draws power from the nodes near each slot [2]. These printers deposit polymer materials, such as polylactic acid (PLA), directly onto modified, configurable GeckoTek unheated build surfaces. The current

*Corresponding author: zsha@austin.utexas.edu

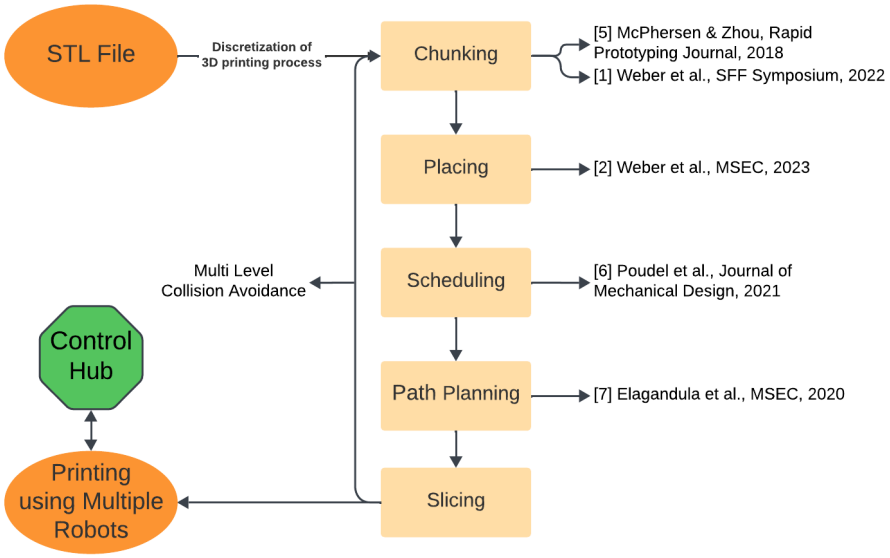

FIGURE 2: A TYPICAL OPEN-LOOP COOPERATIVE 3D PRINTING PROCESS [1]

C3DP system has established methods for geometric partitioning (e.g., chunking), manufacturing scheduling, job placement, and path planning [1].

However, with the autonomy that AM and SM offer, and more specifically C3DP, there is a large need for establishing and improving methodologies for in-situ monitoring of prints. Having an in situ monitoring framework is crucial for scaling up C3DP to large scale and production level printing. Monitoring framework allows manufacturers to receive image data which can be processed for errors providing insights to enhance print quality. To this end, the prior in situ C3DP monitoring frameworks [3, 4] are further improved in this study, using two Intel RealSense D435i Depth Cameras, a custom built heated bed and control system, and a closed-loop algorithm all contained within a 1×2 build surface and opposing printer configuration. This setup, shown in Figure 1, features two printers in an opposing configuration.

The C3DP system, as a whole, relies on dividing large objects into smaller, manageable sections that each printer can handle, a process called “chunking." There are two types of chunking: Z chunking and XY-chunking [1, 2, 5]. After the object is divided, each chunk is assigned a spot on the factory floor, and a schedule is created to ensure that the printers finish their parts as efficiently as possible [6]. Path planning is used to prevent collisions as the printers move around [7]. A typical C3DP process is illustrated in Figure 2.

The C3DP platform is managed through a control hub that can send commands to and receive data from the printers, but currently operates in an open-loop system. Printers can report data such as nozzle temperature, expected position, and print status, while the control hub can send G-code commands to the printers. Although this setup provides operational control, there is no way to externally verify printer actions. This means that the actual nozzle position might differ from the expected position due to poor calibration or even collisions, potentially leading to print failures that the printer cannot detect on its own. We previously developed a monitoring framework for the C3DP system, which detected print failures and communicated with the control hub but required manual intervention to halt faulty prints [3]

Despite using optimized parameters on the C3DP platform, there are still risks of failure, such as extrusion issues, bed miscalibration, warping, and stringing—issues we have encountered in our own tests. Figure 3 shows examples of common FFF defects, like layer splitting and interfacial gaps, which occurred during a cooperative test print of a 3D portrait bust due to a number of factors such as inconsistent extrusion and variance in Z-level calibration. While FFF defects are generally manageable given the low material costs and print times, integrating FFF or advanced methods like C3DP into an automated factory setting will require a system to ensure accurate, error-free prints to avoid damages to printers and maintain cost-efficiency and timely production.

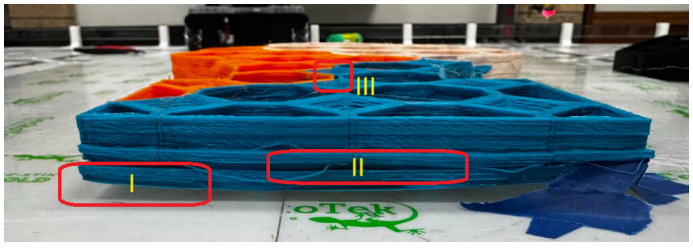

FIGURE 3: COMMON ISSUES IN C3DP. (I) WARPING, (II) LAYER SPLITTING, AND (III) INTERSTITIAL GAPS

This work aims to expand on this methodology by incorporating a closed-loop feedback system to mitigate print errors and defects in real-time without halting the build. In particular, this study focuses on three types of defects in C3DP: 1) warping & layer splitting, and 2) interstitial gaps. To handle the warping issues that are commonly seen in large-format print, we developed a computer vision-based in-situ monitoring system along with a closed-loop heated bed control system. In C3DP, discrete,

feedback-driven control over the heated bed enables optimizing build surface conditions in multi-material applications for high part quality, prevents excess energy consumption and heat generation as the platform scales. The computer vision-based in situ monitoring can also support the detection of interstitial gaps while the closed-loop system for error correction is realized through the control of robotic arms for real-time position compensation. These two in situ monitoring and closed-loop systems serve as a demonstrator of future closed-loop hardware integrations.

The remaining sections are organized as follows: First, we survey existing literature to validate the current research gaps in in-situ monitoring. Next, we briefly discuss existing open-loop computer vision systems and recent modifications to those frameworks, mainly in the image augmentation and matching approaches for optimized edge detection. Then, we detail our approach to implement closed-loop feedback through the improved algorithm and heated bed control system. Finally, we analyze the results of the print quality improvements seen with closed-loop feedback control of build surface temperature and discuss the future work associated with this project.

2. RELEVANT LITERATURE

Process monitoring in additive manufacturing (AM) is an active research area due to the variability in part quality, which is a notable drawback of the process. This issue is especially critical for metal AM, where industries like aerospace require parts to meet strict quality standards that are challenging to verify with AM methods [8]. Consequently, extensive monitoring and control techniques are being explored to ensure that additively manufactured parts are defect-free and meet these high standards. For example, industrial solutions like EOS Smart Monitoring adjust parameters like laser power during builds to meet quality specifications [9].

For FFF printing, however, this level of quality assurance is generally unnecessary, as parts are typically not used in such demanding applications. Still, FFF has a higher failure rate, around 20% for unskilled users [10]. As a result, much research has been done in process monitoring for FFF printing, with 2D vision being the most explored method [11, 12]. For instance, deep learning methods with live camera capture have been used to track, detect, and correct extrusion errors from the nozzle [13, 14]. Like the setup used in this research, externally mounted cameras can watch the printed object and compare the image to the STL file [15]. Moreover, 2D vision techniques can be applied layer by layer and compared to the relevant step in the G-code [16]. These external cameras are capable of detecting warping, stringing, and other printing defects using machine learning (ML) methods [17, 18].

The most prevalent gaps in AM process monitoring are the lack of accurate in-situ defect detection and the capability of real-time correction to adequately improve final part quality. Our prior work sought to tackle the first of these gaps by improving the image-processing methodologies for more accurate defect detection and characterization through Canny edge detection and data augmentation yielding a larger, more diverse image training dataset. Moreover, our previous work enhanced the ML methodology of error detection using image augmentation whereas previous ML methods for stringing and warping detection were proven ineffective in testing and in situ monitoring [4, 18].

The second research gap, which focuses on quantifying improvements in final part quality through feedback control, has established methods in closed-loop controller logic but limited quantitative analysis of final part quality based on these logic inputs and outputs. Numerous approaches for closed-loop monitoring in FFF have used fuzzy logic to modulate parameters such as nozzle and bed temperature based on image data of in-process prints, but analysis of final parts is predominantly qualitative or simulation-based [19, 20]. Moreover, in the context of large-scale, forward deployable manufacturing environments, such as the C3DP system, data driven approaches are preferred over fuzzy logic controllers for more computationally efficient ML algorithms, to which our framework is specifically adapted." [21]. Figure 4 shows the addition of the closed-loop monitoring system to our existing framework and ML-driven defect detection.

3. C3DP MONITORING FRAMEWORK

Prior to discussing the methodology of warping, layer-splitting, and interstitial gap detection in a closed-loop system, we first need to reevaluate the gaps in the current C3DP process monitoring framework. The current C3DP monitoring framework utilizes one camera for image matching and stringing detection. The logic of the program is shown in Figure 4. With this current framework being the second attempt at in-situ monitoring, real-time data processing was unsuccessful. Moreover, even with a more confident stringing detection using a machine learning model, the results were aporetic given various part geometries. With that, we have outlined in Figure 4 the enhancements made to the framework by applying real-time layer by layer Canny edge detection. Lastly, the original framework utilized the structural similarity index measure (SSIM) for image matching, which a lot of times outputs incorrect values [4]. Therefore, in this methodology, SSIM is not used and other methods are explored to compare the edge detected contours (see Section 3.3).

Figure 5 illustrates an overview of the hardware of the computer vision-based in-situ monitoring and error detection, as well as the closed-loop heated bed system. In the following subsections, we introduce our new methodology, including both hardware and software, for the detection of warping (including layer splitting) and interstitial gap, along with the closed-loop feedback control.

3.1. Heated Bed Setup and Control

To ease integration into the modularity of the C3DP platform and to maintain design simplicity, the heated bed was assembled entirely from off-the-shelf (OTS) components that are normally found on commercially available FFF systems and was designed to be retro-fit onto the existing GeckoTek build surfaces used on the current C3DP platform. The heated bed is controlled via an Arduino Uno, which sends PWM signals to a solid-state relay that controls the power output of the AC to DC power supply to modulate the bed temperature.

$$\frac{1}{T} = \frac{1}{T_0} + \frac{1}{B} \ln\left(\frac{R}{R_0}\right) \tag{1}$$

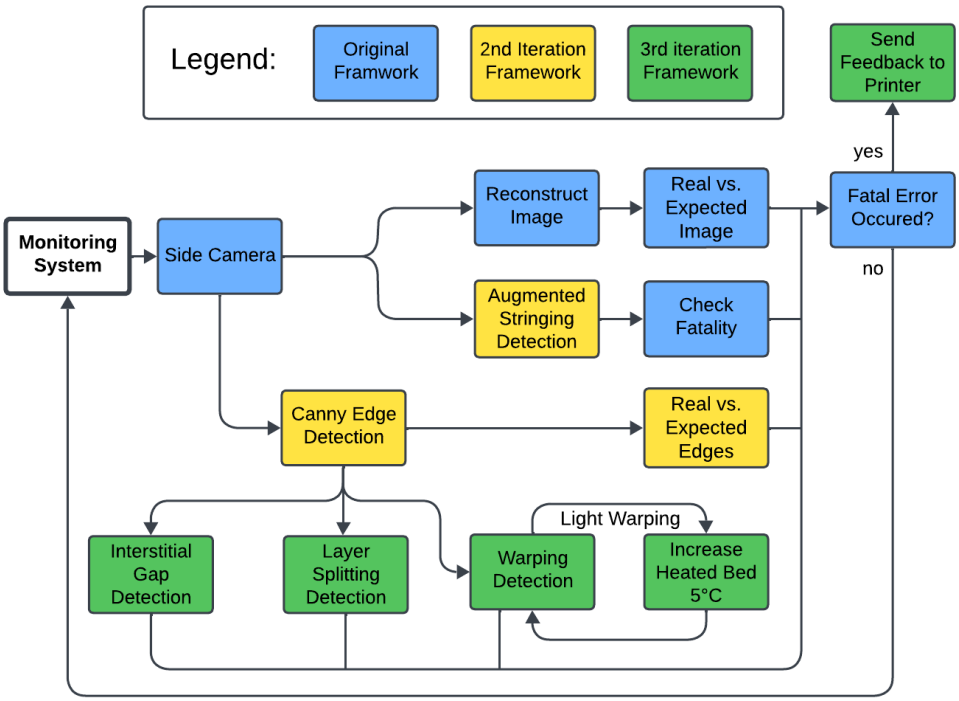

FIGURE 4: AN ENHANCED C3DP MONITORING FRAMEWORK

TABLE 1: HEATED BED COMPONENTS AND THEIR PURPOSES

NUMBER	ITEM	PURPOSE
1	Creality 235mm x 235mm Aluminum Base & Glass Build Surface	Build surface
2	24V 30A AC-DC Power Supply Unit	Main power to system
3	Arduino Uno	Main system controller
4	Keenovo 235mm x 235mm Silicone Heating Array, 660W	Heating element
5	OMRON Solid State Relay	Control between Arduino and Heating element
6	M4 10mm Standoffs (x4)	Mounting to GeckoTek plate
7	M4 countersunk screws	Mounting build surface to standoffs
8	18 AWG Wire	Circuit wiring
9	Resistors (10kOhm, 4.7kOhm)	Voltage divider for thermistor

The temperature value is acquired and read by the Arduino via analog input, which is provided by a thermistor in the heated bed. This thermistor was calibrated empirically to acquire its beta value, the physical parameter that models its temperature-resistance response. The Steinhart-Hart equation (see Eq. (1)) is used to calculate current temperature reading in degrees Celsius, and is driven by the beta value and resistance measurement provided from an integrated voltage divider.

By setting outputs to the relay, the Arduino can command a new target temperature value as well by modulating the PWM signals, and Eq. 1 can be used to confirm the target temperature has been reached and will continue to send signals to the relay to hold this temperature within 2 degrees of the target value. This control system can be directly controlled via PySerial, a readily available Python library, for robust closed loop monitoring based on computer-vision triggered inputs. Table 1 shows the bill of materials (BOM) for the components used in the heated bed setup, and Figure 6 shows the individual labeled components of the heated bed after full assembly and configuration.

Since the heated bed is a direct modification to the traditional C3DP build surface, the bed mesh leveling calibration had to be adjusted to account for the increased Z height of the new heated bed surface, as well as the new reference XY coordinate frame of the printers. The new printing bounds for the heated bed were manually confirmed, and the C3DP bed mesh leveling macro-function was able to create a bed-mesh map for both printers in their opposing configurations. Minor modifications were made to the Z-homing sequence in the G-code so that the BL-Touch homing probe would touch-off the heated bed plate, not the lower height GeckoTek plate.

The test parts used were sliced in Cura 5.6.0, and the existing C3DP profile was modified to fit the opposing printer configuration (300 mm x 600 mm build surface) and increased Z-height of the build surface for the heated bed prints. The XY position of

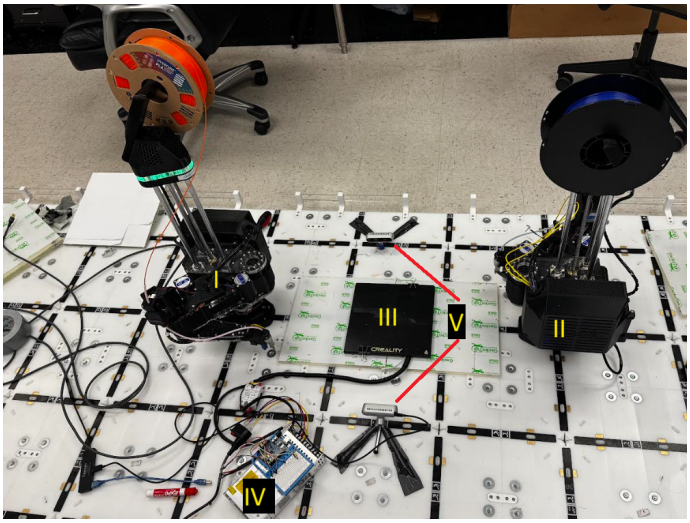

FIGURE 5: C3DP HEATED BED CONFIGURATION. (I) SCARA ROBOT 1, (II) SCARA ROBOT 2, (III) HEATED BED BUILD SURFACE, (IV) HEATED BED CONTROL SYSTEM, AND (V) REAL SENSE DEPTH CAMERAS.

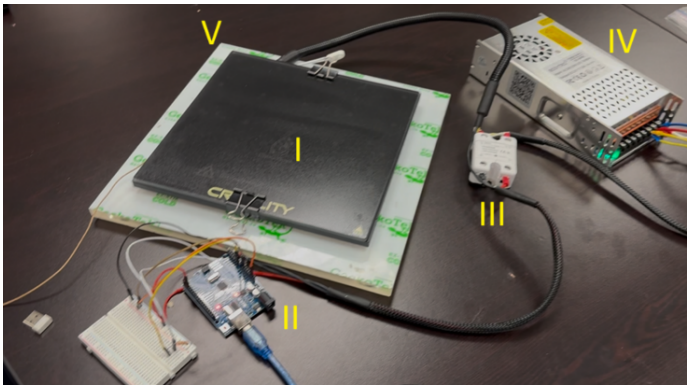

FIGURE 6: LABELED COMPONENTS OF HEATED BED. (I) HEATED BED WITH GLASS SURFACE, (II) ARDUINO UNO AND PRIMARY CIRCUIT, (III) SOLID STATE RELAY, (IV) POWER SUPPLY UNIT, AND (V) MODIFIED GECKOTEK BUILD PLATFORM

the parts was manually calculated and adjusted to ensure accurate positioning and orientation of the part on the build surface during cooperative prints.

In this study, we use discretized heated bed control rather than a constantly activated system. Each print chunk can thus have independent heating activation based on real-time defect signals of the active printing part. The benefits are primarily for multi-material C3DP applications and energy savings. Certain thermoplastics in FFF, such as PLA, print optimally with higher bed temperatures around $60^{\circ}C$, while other materials, such as chlorinated polyethylene (CPE), print optimally with minimal to no heat input. When printing multi-material parts using C3DP, a discretized control system works when part quality and mechanical strength of interface joints are of the most importance. Similarly, as parts grow in Z height during a print, the increased thermal mass affects the temperature distribution throughout the part and is very geometry and material dependent. Although this effect is usually minimal in typical FFF applications, automated microstepping of the temperature values can greatly benefit when quality is a key factor.

A second benefit of discretized control of the heated bed is energy savings, especially when the scale of the system is considered. For reference, a single heated bed system draws around 675W at peak power, and this scales to over 4kW of power draw on a system with only six robots if the heated beds were constantly activated. The idea behind C3DP is to have modular, autonomous, efficient factories with any number of manufacturing robots. Therefore, specific circumstances, such as material usage, build size, and machine utilization, should be considered when evaluating the number of systems that can be scaled to keep the manufacturing process cost and energy efficient.

3.2. Image Processing

To address the gap in proper detection of part boundaries in existing nascent in situ monitoring frameworks, Canny edge detection is utilized to extract coordinates of contours in the part. This is an important step in image processing because it affects how well errors are detected. First, the images are converted from red-blue-green (RBG) to hue-saturation value (HSV). It is important to note that the parts are masked based on the color of the filament. Therefore, HSV supports color separation (i.e. separates color information (hue) from intensity (value)), various lighting conditions, simplified thresholding, and improved edge detection (i.e. the value parameter in HSV represents brightness allowing for clearer edges). Second, the image is blurred to remove any glare or lighting differences in the image. The blur is applied using a Gaussian filter with kernel size empirically tuned based on visual reduction in glare. Third, Canny edge detection is applied to the image, and an array of coordinates of all edges is saved. These edges then run through a morphological and Hough Lines transformation to get clearer edges and straighter lines.

After the edge detection algorithm, the coordinates in the array of edges are compared against each other to determine the largest and outermost edge. This outermost contour is then processed to detect defects in C3DP. In the next subsections, we discuss how we take this contour and create insights on warping, layer splitting, and interstitial gaps that can then be communicated to the printers for data-driven decision-making.

3.3. Warping and Layer Splitting Detection

Warping and layer splitting are major defects found in C3DP. We detected these defects in a truly in situ layer-by-layer process. Every two millimeters, an image is taken and saved to a directory. The metric of every two millimeters was chosen based on prior observed errors in cooperative prints where we found two millimeters as a common magnitude of interstitial gaps caused by XY misalignment. The framework could be extended to detect smaller gaps, like 1 mm, with higher resolution imaging. These images are useful for human verification and documentation of prints, while also serving as data for the warping and layer-splitting detection algorithm. After the first image, the next image cuts its height down to the first image, and the contours are compared to determine if there is any difference. Various

methods were used to determine the best comparison algorithm and see which yielded the most consistent results. These various methods include bounding edge comparison, closest point comparison, corner point comparison, and K-nearest neighbor (KNN) regression comparison.

The boundary edge comparison looks at the four edges of the two images to see any differences in pixels. Closest-point comparison overlaps the two images, finds the closest point between the two contours, and outputs the max distance in pixels between those points. The corner point comparison finds the corners of the contours and outputs the distance in pixels between those corners. Finally, the last method tested is a statistical approach in which the nearest point is predicted using a K-nearest neighbor regression model that produces clearer contours, and thus should theoretically produce more refined differences. Using these methods, thresholds are determined for either increasing the heated bed (i.e. light warping or layer splitting) or stopping the print, should a fatal warping or layer splitting be detected.

3.4. Interstitial Gap Detection

Another common defect found in C3DP from the previous literature and our experience is an interstitial gap between two chunks as a result of improper XY calibration. Similarly to warping and layer splitting, Canny edge detection is used to detect the interstitial gap. After the image processing steps described in Section 3.2, the contours of both parts are extracted and compared on a y-axis basis. In other words, for every y value, the farthest x coordinate on the right chunk is compared to the closest x coordinate on the left chunk. This coordinate-by-coordinate process ensures that proper detection is achieved regardless of geometry. Furthermore, similar to the cut-height functionality of the warping and layer splitting, the image masks of each print are cut to the highest y axis of the shorter chunk. This refers to cropping the newer image to the vertical height of the previous image to ensure consistent comparison zones. Finally, another detection technique used from the warping and layer-splitting methodology is the two millimeters imaging. This allows one image to be taken for all error detection. Every two millimeters, an image is taken and run through both the warping and layer splitting algorithm as well as the interstitial gap algorithm.

To validate this method, a print that is purposefully given a two millimeter gap is printed alongside a chunk, and a print that matches perfectly is also printed to see how the algorithm works. The two millimeter gap is chosen because our previous test cases and research have shown this to be the general dimension of an interstitial gap, so our algorithm is successful if it can detect at that level of error. Finally, if a gap is detected, the print is halted and can be recalibrated accordingly.

4. EXPERIMENTS AND RESULTS

A simple geometry of a rectangular prism with dimensions of 100 mm L × 15 mm W × 25 mm H is used as a test case for all the error detection algorithms. This geometry being a long rectangular prism with sharp edges is highly prone to warping. Since warping is simply layer splitting at the base instead of mid-part, we focus on testing warping in the experiment. In the case of layer splitting, the in-situ monitoring and error detection part of the algorithm will not change. For the closed-loop system, instead of increasing the heated bed temperature, the print would halt, allowing for manual intervention to clean off the split layer and revert the G-code file to the layer that faltered.

4.1. Warping Detection

For warping detection, images are captured every two millimeters and saved to a separate image directory within the framework directory. This file management is crucial because these images are then run through image processing to produce an array of the outermost contours, which will then be processed through each of the warping methods described previously.

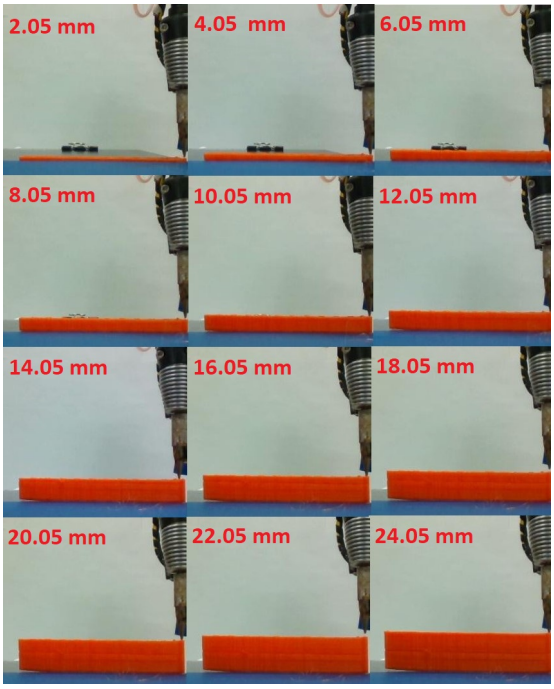

FIGURE 7: IMAGES CAPTURED EVERY 2 MM FOR WARPING DETECTION

Specifically, every image after the first 2.05 mm image is cropped to and compared against its previous image. Before presenting the results of the real-time data processing, we show some visual hypotheses from the images in Figure 7. It is evident that at 10.05 mm the warping begins, but is not very visible, but at 12.05 mm the warping is quite apparent. From then on, the warping does not increase significantly until 24.05 mm.

It was determined earlier prior to in-situ analysis that corner point comparison would be the best method. These thresholds were empirically determined based on repeated test prints and visual confirmation of where warping became noticeable (15 px) and where it caused part failure (35 px). We determined these thresholds by completing prior tests against existing 3D printed parts that had interstitial gaps. For this case in Figure 7, and its associative data in Table 2, all methods were tested in-situ to see if they work any better. It was further proved that corner point comparison is the best method for in-situ analysis. Agreeing with the visual hypothesis from the images that at 10.05 mm warping begins and then continues at 12.05 mm, Figure 8 graphically

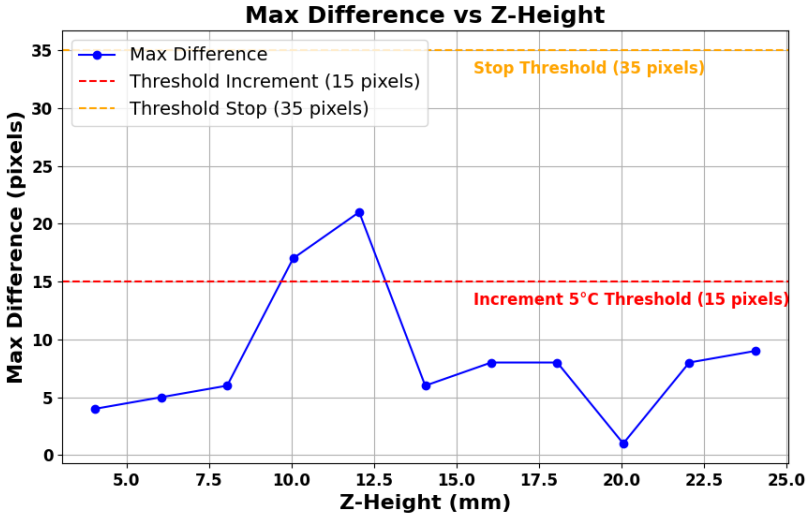

FIGURE 8: CORNER POINT COMPARISON WARPING VS. Z-HEIGHT

TABLE 2: Z-HEIGHT, CORNER POINTS, CLOSEST POINTS, BOUNDING EDGES, AND KNN REGRESSION

Z-Height	Corner Point	Closest Point	Bounding Edges	KNN Regression
4.05 mm	4px	17px	0px	0.08
6.05 mm	5px	129px	129px	2.1
8.05 mm	6px	20px	0px	0.46
10.05 mm	17px	27px	0px	0.3
12.05 mm	21px	20px	0px	0.05
14.05 mm	6px	23px	0px	0.3
16.05 mm	5px	137px	137px	4.78
18.05 mm	8px	17px	0px	0.82
20.05 mm	1px	18px	0px	0.91
22.05 mm	8px	19px	0px	0.55
24.05 mm	9px	28px	0px	0.63

shows how warping increases until the increment threshold of 15 pixels and then shoots down showing a decrease in warping effect.

The potential reasons for the nearest point, bounding edge, and KNN comparison methods not working well could be improper masking of the nozzle, delayed camera capture, and code logic. On a standalone basis, each of these methods worked when an image of a completed part was taken, and then a corner of it was erased artificially. However, for in situ analysis, each of these methods produced significant outliers and bounding edges simply did not work. It is also important to note that corner point comparison may be less effective for geometries with minimal corners or with irregular, organic contours, but we believe that at least the corners of the interstitial boundary would get detected

Sometimes there can be a very unnoticeable delay in image capture due to data loss, which all occurs within the time that the nozzle is changing to the next layer. Even though the nozzle always appears justified to the right where the nozzle z height increases for the next layer, there is about a second delay for the next layer to start. This is significant because the camera could take an image anytime in that delay, causing errors that are not explainable in all warping detection methods. As corner point comparison only looks at the vertices of the edges, proper focus is not significant, and this makes this method the best suited. This issue needs to be addressed because the quality of every image is not the same. Potential solutions to improve these failed methods and have more consistent results from corner point comparison will be discussed in further detail in Section 5. However, since corner point comparison shows the most alignment with our visual hypothesis, this method is used for the overall framework.

4.2. Interstitial Gap Detection

The last common error found in C3DP is an interstitial gap between the chunks due to improper calibration. The goal here is to detect a gap using edge detection and recalibrate the printer in a closed-loop control system. In our first attempt at interstitial gap detection, a feasibility test was conducted. That means we simply detect a high gap threshold and stop the print if the gap is larger than a set threshold. This process will prove that gap detection is working and closed-loop feedback is possible.

Using the same geometry of the test case for warping and layer splitting but separating it into two chunks by splitting the rectangular prism at a 60 degree angle, the interstitial gap detection test is a cooperative print with a camera looking at both chunks to create individual masks for y-axis-based comparison of the gaps. These gap distances in image pixels can then be graphed to show increasing or decreasing gap growth, which can be useful for non-in situ, post-processing analysis. For this case of graphically representing gap growth, a part was printed with a unique geometry where the second chunk was printed with a significant gap initially and then slowly reduced to no gap.

As seen in the graph in Figure 10, the gap is initially very high and decreases as it increases in height. This graph assumes

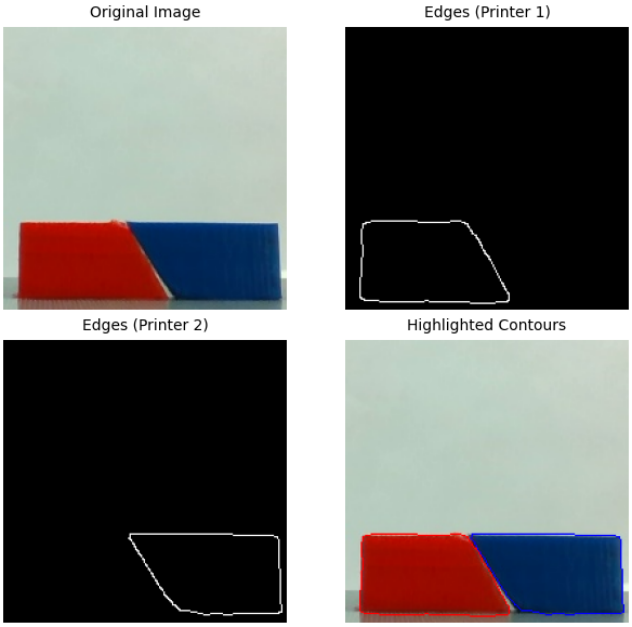

FIGURE 9: C3DP GRADIENT GAP

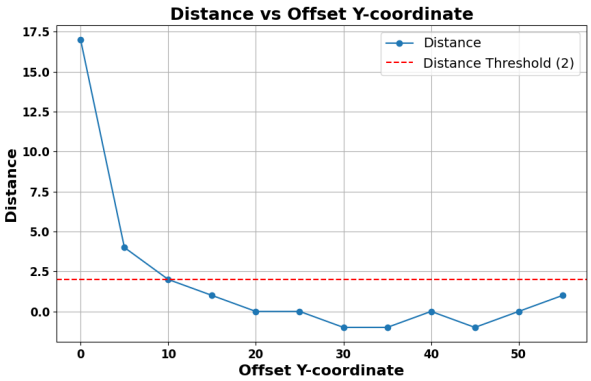

FIGURE 10: GRADIENT GAP DISTANCE GRAPH

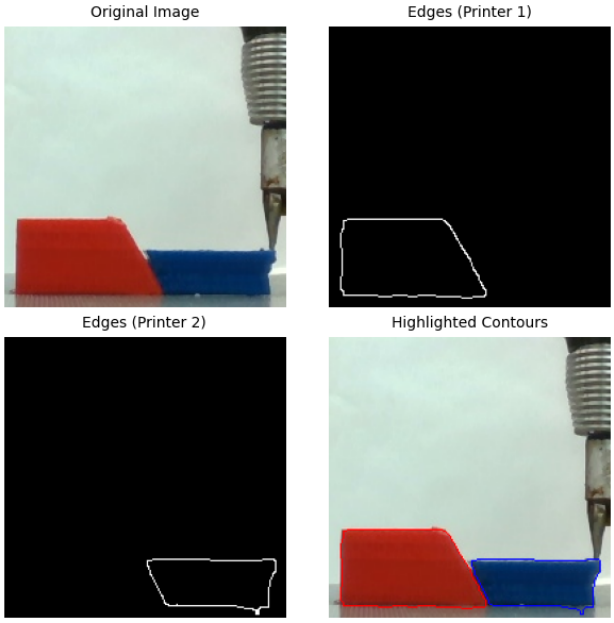

FIGURE 11: C3DP INDUCED GAP

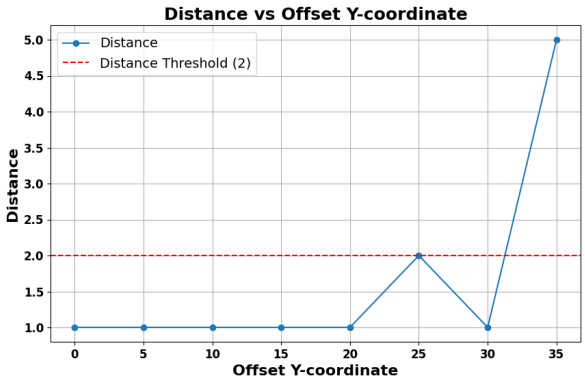

FIGURE 12: INDUCED GAP DISTANCE GRAPH

that the very bottom of the boundary is the y = 0 coordinate and then increases from there. The points are determined by taking standardized steps to speed up the processing of this graph. The iterative logic for the interstitial gap detection would go through pixel by pixel and compare the last and first x coordinates of the first and second printers, respectively. Therefore, graphing every point would take a long time, and the program often crashes. As a result, the gap is reasonably graphed step by step.

The next test case is to prove closed-loop feedback where the printer will stop when a gap is detected. The simplest way to prove this is to artificially induce a gap mid-print by manually moving the print bed. Looking at Figure 5, we used binder clips to hold a glass plate on top of the heating element listed in Table 1. Given that this glass plate is not permanently fixed, we printed one chunk, and then while the second chunk was printing, we slowly moved the glass plate on top of the heated element to induce the gap. This process works successfully, as shown by the images in Figure 11 and Figure 12 showing the increase of the gap until it surpasses the distance threshold of 2 pixels at which point the monitoring framework sent a pause command in G-code. This threshold was determined through iterative testing with already printed parts. The monitoring framework in this section is the fully coded system where warping detection, closed-loop heated bed control, interstitial gap detection, and printer communication to stop printing are all running actively.

5. CONCLUSION AND FURTHER WORK

Overall, this monitoring framework is successful in collecting and processing image data to detect warping and interstitial gaps. In addition, closed-loop control of the heated bed successfully reduced warping effects. We can also show that closed-loop communication with the printer is possible by sending G-code commands. This allows for future work on closed-loop printer calibration. There are a few gaps that need to be addressed in the next iteration of this in-situ monitoring framework. We need to determine accurate image capture techniques to consistently capture clear and focused photos. This could be done by cropping

out the nozzle from the image and only capturing the part.

This study focused on demonstrating feasibility in controlled conditions, but robustness to intensity variation and noise in large-scale production environments is an important area for future work. Data ablation studies were not conducted, but we agree that evaluating the algorithm's tolerance to lighting or background variation would improve its applicability.

While the in situ monitoring framework presented in this paper lays a thorough foundation for improving C3DP and various other forms of AM, it is limited in that it relies only on external datasets from images captured during the printing process. To incorporate a robust closed-loop process monitoring system, these *extrinsic* data must be paired and correlated with direct machine data (*intrinsic* data) in order to paint the full picture of what is happening during the manufacturing process. Extrinsic data includes, and is not limited to, computer vision systems, external sensors, and processing stations associated with the machine. Intrinsic data, on the other hand, includes and is not limited to positional data from machine encoders, temperature data from the nozzle, and motion data (velocity, acceleration, and jerk) from the motors. By capturing the full breadth of this data, we can begin to build a large dataset that can draw correlations between these parameters and the part being manufactured, and further workflows can be developed to incorporate redundancy systems, ML models to predict final part quality, and construct digital twins of the factory environment. The challenges in this workflow include capturing and filtering only relevant data, time-synchronizing all datasets, storing and processing the data computationally and effectively, and building an accurate ML model with enough capabilities to expand to other forms of AM through transfer learning.

ACKNOWLEDGMENTS

This work was partially supported by the Army Research Lab (ARL) via grant number W911NF-24-2-0007. Any opinions, findings, conclusions, or recommendations expressed in this material are those of the authors and do not necessarily reflect the views of ARL.

REFERENCES

[1] Weber, Daniel, Zhou, Wenchao and Sha, Zhenghui. "Job Placement for Cooperative 3D Printing." *Manufacturing Science and Engineering Conference (MSEC)*. New Brunswick, NJ, June 12–16, 2023. DOI 10.1115/MSEC2023-104613. URL https://doi.org/10.1115/MSEC2023-104613.

[2] Weber, Daniel, Zhou, Wenchao and Sha, Zhenghui. "Z-Chunking for Cooperative 3D Printing of Large and Tall Objects." *Proceedings of the 33rd Annual International Solid Freeform Fabrication Symposium (SFF)*. Austin, TX, July 25–27, 2022. DOI 10.26153/tsw/44190. URL http://dx.doi.org/10.26153/tsw/44190.

[3] Mensch, Cole, Swaminathan, Anuj and Sha, Zhenghui. "A real time monitoring framework for cooperative 3D printing." *Proceedings of the 35th Annual International Solid Freeform Fabrication Symposium (SFF)*. Austin, TX, August 11–14, 2024. URL https://utw10945.utweb.utexas.edu/2024-table-contents.

[4] Sanam, Harshin and Sha, Zhenghui. "Enhancing In-Situ Monitoring Framework of Cooperative 3D Printing via Edge Detection and Image Augmentation." *International Manufacturing Science and Engineering Conference (MSEC)*. Greenville, South Carolina, June 23–27, 2025.

[5] McPherson, Jace and Zhao, Wenchao. "A chunk-based Slicer for cooperative 3D printing." *Rapid Prototyping Journal* Vol. 25 No. 9 (2018): pp. 1436–1446. DOI 10.1108/rpj-07-2017-0150.

[6] Poudel, Laxmi, Zhao, Wenchao and Sha, Zhenghui. "Resource constrained scheduling for multi-robot cooperative three dimensional printing." *Journal of Mechanical Design* Vol. 143 No. 7 (2021). DOI 10.1115/1.4050380.

[7] Elagandula, Saivipulteja, Poudel, Laxmi, Sha, Zhenghui and Zhao, Wenchao. "Multi-robot path planning for cooperative 3D printing." *International Manufacturing Science and Engineering Conference (MSEC)*. Virtual, September 3, 2020. DOI 10.1115/msec2020-8390. URL https://doi.org/10.1115/msec2020-8390.

[8] Usha, S. "In situ monitoring of Metal Additive Manufacturing Process: A Review." *Additive Manufacturing* (2021): pp. 275–299DOI 10.1016/b978-0-12-822056-6.00007-2.

[9] "Eos Smart Monitoring for 3D printing." EOS. URL https://www.eos.info/en-us/enablement/software/eos-smart-monitoring.

[10] Wittbrodt, Ben T., Glover, Adam G., Laureto, Joshua, Anzalone, Gerald C., Oppliger, Douglas, Irwin, John L. and Pearce, Joshua M. "Life Cycle Economic Analysis of distributed manufacturing with open-source 3-D printers." *Mechatronics* Vol. 23 No. 6 (2013): pp. 713–726. DOI 10.1016/j.mechatronics.2013.06.002.

[11] Fu, Yajun, Downey, Andrew, Yuan, Lijing, Pratt, Andrew and Balogun, Yetunde. "In situ monitoring for fused Filament Fabrication Process: A Review." *Additive Manufacturing* Vol. 38 (2021): p. 101749. DOI 10.1016/j.addma.2020.101749.

[12] Oleff, Alexander, Küster, Benedikt, Stonis, Max and Overmeyer, Ludger. "Process monitoring for material extrusion additive manufacturing: A state-of-the-art review." *Progress in Additive Manufacturing* Vol. 6 No. 4 (2021): pp. 705–730. DOI 10.1007/s40964-021-00192-4.

[13] Brion, Daniel A. and Pattinson, Sebastian W. "Generalisable 3D printing error detection and correction via multi-head neural networks." *Nature Communications* Vol. 13 No. 1 (2022). DOI 10.1038/s41467-022-31985-y.

[14] Jin, Zhi, Zhang, Zhipeng and Gu, Guo-Xing. "Autonomous in-situ correction of fused deposition modeling printers using computer vision and Deep Learning." *Manufacturing Letters* Vol. 22 (2019): pp. 11–15. DOI 10.1016/j.mfglet.2019.09.005.

[15] Straub, Jeremy. "Initial work on the characterization of Additive Manufacturing (3D printing) using software image analysis." *Machines* Vol. 3 No. 2 (2015): pp. 55–71. DOI 10.3390/machines3020055.

[16] Petsiuk, Alexey L. and Pearce, Joshua M. "Open source computer vision-based layer-wise 3D printing analysis." *Additive Manufacturing* Vol. 36 (2020): p. 101473. DOI 10.1016/j.addma.2020.101473.

[17] Brion, Daniel A. J., Shen, Mingze and Pattinson, Sebastian W. "Automated recognition and correction of warp deformation in extrusion additive manufacturing." *Additive Manufacturing* Vol. 56 (2022): p. 102838. DOI 10.1016/j.addma.2022.102838.

[18] Paraskevoudis, Konstantinos, Karayannis, Panagiotis and Koumoulos, Elias P. "Real-time 3D printing remote defect detection (stringing) with Computer Vision and artificial intelligence." *Processes* Vol. 8 No. 11 (2020): p. 1464. DOI 10.3390/pr8111464.

[19] Qin, Wang et al. "Research on Process Control of 3D Printing Technology Based on Multi-Sensor Technology." *2020 IEEE 3rd International Conference of Safe Production and Informatization (IICSPI)*: pp. 675–679. 2020. DOI 10.1109/IICSPI51290.2020.9332336.

[20] Liu, Chenang et al. "Image Analysis-Based Closed Loop Quality Control for Additive Manufacturing with Fused Filament Fabrication." *Journal of Manufacturing Systems* Vol. 51 (2019): pp. 75–86. DOI 10.1016/j.jmsy.2019.04.002.

[21] Mumali, Fredrick and Kałkowska, Joanna. "Intelligent Support in Manufacturing Process Selection Based on Artificial Neural Networks, Fuzzy Logic, and Genetic Algorithms: Current State and Future Perspectives." *Computers Industrial Engineering* Vol. 193 (2024): p. 110272. DOI 10.1016/j.cie.2024.110272.